



Performance of a Deep Learning Algorithm for Automated Segmentation and Quantification of Traumatic Pelvic Hematomas on CT

David Dreizin¹ · Yuyin Zhou² · Yixiao Zhang² · Nikki Tirada³ · Alan L. Yuille⁴

© Society for Imaging Informatics in Medicine 2019

Abstract

The volume of pelvic hematoma at CT has been shown to be the strongest independent predictor of major arterial injury requiring angioembolization in trauma victims with pelvic fractures, and also correlates with transfusion requirement and mortality. Measurement of pelvic hematomas (unopacified extraperitoneal blood accumulated from time of injury) using semi-automated seeded region growing is time-consuming and requires trained experts, precluding routine measurement at the point of care. Pelvic hematomas are markedly variable in shape and location, have irregular ill-defined margins, have low contrast with respect to viscera and muscle, and reside within anatomically distorted pelvises. Furthermore, pelvic hematomas occupy a small proportion of the entire volume of a chest, abdomen, and pelvis (C/A/P) trauma CT. The challenges are many, and no automated methods for segmentation and volumetric analysis have been described to date. Traditional approaches using fully convolutional networks result in coarse segmentations and class imbalance with suboptimal convergence. In this study, we implement a modified coarse-to-fine deep learning approach—the Recurrent Saliency Transformation Network (RSTN) for pelvic hematoma volume segmentation. RSTN previously yielded excellent results in pancreas segmentation, where low contrast with adjacent structures, small target volume, variable location, and fine contours are also problematic. We have curated a unique single-institution corpus of 253 C/A/P admission trauma CT studies in patients with bleeding pelvic fractures with manually labeled pelvic hematomas. We hypothesized that RSTN would result in sufficiently high Dice similarity coefficients to facilitate accurate and objective volumetric measurements for outcome prediction (arterial injury requiring angioembolization). Cases were separated into five combinations of training and test sets in an 80/20 split and fivefold cross-validation was performed. Dice scores in the test set were 0.71 (SD ± 0.10) using RSTN, compared to 0.49 (SD ± 0.16) using a baseline Deep Learning Tool Kit (DLTK) reference 3D U-Net architecture. Mean inference segmentation time for RSTN was 0.90 min (± 0.26). Pearson correlation between predicted and manual labels was 0.95 with $p < 0.0001$. Measurement bias was within 10 mL. AUC of hematoma volumes for predicting need for angioembolization was 0.81 (predicted) versus 0.80 (manual). Qualitatively, predicted labels closely followed hematoma contours and avoided muscle and displaced viscera. Further work will involve validation using a federated dataset and incorporation into a predictive model using multiple segmented features.

Keywords Pelvic fractures · Pelvic ring disruptions · Computed tomography (CT) · Hematoma volume · Segmentation · Deep learning · Artificial intelligence (AI) · Computer-aided diagnosis (CAD) · Convolutional neural network (CNN) · Fully convolutional network (FCN) · Recurrent saliency transformation network (RSTN)

✉ David Dreizin
daviddreizin@gmail.com

Yuyin Zhou
zhouyuyiner@gmail.com

Yixiao Zhang
yzhan334@jhu.edu

Nikki Tirada
pmeteesat@gmail.com

Alan L. Yuille
alan.l.yuille@gmail.com

¹ Department of Diagnostic Radiology and Nuclear Medicine & R Adams Cowley Shock Trauma Center, University of Maryland School of Medicine, Baltimore, MD, USA

² Computational Cognition, Vision, and Learning (CCVL), Johns Hopkins University, Baltimore, MD, USA

³ Department of Diagnostic Radiology and Nuclear Medicine, University of Maryland School of Medicine, Baltimore, MD, USA

⁴ Computational Cognition, Vision, and Learning (CCVL), Johns Hopkins University, Baltimore, MD, USA

Introduction

Arterial hemorrhage associated with pelvic fractures is a leading but reversible cause of death following blunt trauma, with mortality rates of 5–15% in initially hemodynamically stable patients [1, 2] and up to 54% in patients with initial hemodynamic compromise [3–5]. Early detection of arterial hemorrhage at contrast-enhanced CT promotes timely intervention, typically with angioembolization [6]. Objective and accurate radiologist prediction of major arterial bleeding is challenging. Active arterial extravasation may be intermittent for a variety of reasons, including episodic vascular thrombosis, hypotension, tamponade, and vessel spasm, and contrast extravasation (CE) may not be present on CT [7]. Several studies have shown that pelvic hematoma volume (i.e., the total amount of accumulated blood in the pelvis from the time of injury to CT), segmented using manual [8] and semi-automated labeling [9], is a highly accurate predictor of the need for angioembolization and correlates with transfusion requirement and mortality. In a multivariable CT prediction model of major arterial injury (including hematoma volume, CE, pelvic fracture patterns, and degree of atherosclerosis), hematoma volume was the strongest predictor [9]. However, manual labeling requires substantial time effort that precludes use at the point of care in a busy trauma referral center setting, while semi-automated region-growing methods are user-dependent and technical proficiency is uncommon. Shorthand diameter-based size estimates have been shown to be inaccurate [10]. Qualitative assessment (e.g., small, moderate, large) is commonly employed in the clinical setting but is highly subjective.

Deep learning using convolutional neural networks (CNNs) has become the most widely used and robust method for image segmentation and classification tasks [11, 12]. CNNs capture low-level multidimensional imaging data from input images by a series of linear operations (filters or kernels). The receptive field of the filter convolves along successive positions of the image matrix to produce feature maps, which serve as the input for deeper convolutional layers. The contracting path of a convolutional neural network employs downsampling (pooling) operations that increase the receptive field of the filter providing global, contextually rich information, but information about local dependencies and fine detail is lost. Both low-level semantic information (e.g., edges, gradients, texture, and intensity) and contextually rich high-level information related to gross structure and location must be preserved for accurate segmentation [13]. Fully convolutional neural networks (FCNs) such as U-Net and V-Net use an expanding path of deconvolutional (upsampling) operations and skip connections which bypass deeper layers to restore anatomic detail lost in the contracting path [14–16], however max-pooling layers, which increase the receptive field of filters allowing learning from large-scale contextual cues, also

cause information loss, result in coarse segmentations [13]. Furthermore, class imbalances inherent to the large datasets of abdominopelvic CT scans result in suboptimal convergence and limit the ability to achieve accurate fine detail segmentations with conventional FCN architectures.

There are numerous applications of CNNs for segmentation of solid organs and masses [17–25], however automatic segmentation of complex free fluid in the abdomen or pelvis poses unique challenges, particularly on CT, and we are not aware of relevant deep learning implementations. Problems specific to the segmentation of traumatic pelvic hematomas include their highly irregular, ill-defined, and intricate contour, variable multi-compartmental location (including along the pelvic sidewalls, suprapubic space, presacral space, and retroperitoneum), anatomic distortion of the fractured pelvis, and closely overlapping attenuation of hematoma with a variety of adjacent structures such as genitourinary and reproductive organs, bowel, and muscles [9, 10, 26, 27]. A successful network architecture requires learning from global contextual information to account for the large scan volume, variable location of hematoma, and positional shifts in the setting of trauma, as well as local dependencies for segmentation of fine contours and weak boundaries. C2F is a tri-planar 2D UNet-based network trained using two identical sequential FCN base architectures in an end-to-end fashion. Initially, a coarse-scaled network is applied to the entire volume to localize smaller volumes of interest from axial, coronal, and sagittal images. The smaller volume is encapsulated with bounding boxes and cropped, then fine-scaled networks are applied. This method has been successfully employed for segmentation of the pancreas on CT—a task which faces similar challenges related to the small size of the organ with respect to the imaged volume, low contrast with adjacent anatomy, fine lobulated margins, and variable position [23]. A recent state-of-the-art modification of C2F (the recurrent saliency transformation network—RSTN) further improves fine contour extraction (saliency) of the pancreas target [28]. In this work, we demonstrate the feasibility of RSTN as a solution for segmentation and volumetric analysis of pelvic hematomas which occupy a relatively small proportion of an entire trauma CT volume, vary in location, are susceptible to positional shifts from pelvic ring distortion, and have weak boundaries.

CT Data and Ground Truth Labeling

The work is part of an IRB-approved and HIPAA-compliant study. The de-identified dataset consisted of chest, abdomen, and pelvis trauma CT scans routinely acquired in the arterial phase from 253 patients (144,881 images) with pelvic ring fractures, and hematoma volumes greater than 30 ml (1/10th of one unit of blood) [29]. Patients with small hematomas (less than 80–200 mL) are considered at negligible to small risk for major arterial bleeding and would warrant conservative

management [8, 9]. Our dataset included a substantial number of patients in a low range (Fig. 1) to ensure a successful algorithm would have the intrinsic ability to assist decision-making by discriminating patients that would require observation alone from those with progressively higher likelihood of requiring intervention. Baseline patient characteristics included mean age of 49.6 (standard deviation (SD) \pm 19.7), gender distribution (70% male, n = 178; 30% female, n = 75), mean injury severity score (ISS) of 26.5 (SD \pm 13.9), and mean pelvic-extremity abbreviated injury scale (AIS) score of 3.0 (SD \pm 0.79). Using the Tile classification for pelvic instability (A—mechanically stable, B—rotationally unstable, and C—globally unstable), 110 patients (42%) had mechanically stable (Tile A) pelvic fractures, 83 patients (33%) had rotationally unstable (Tile B) pelvic fractures (associated with distortion primarily in the x- and y-axes), and 60 patients (24%) had globally unstable (Tile C) pelvic fractures (associated with severe distortion in x-, y-, and z-axes). A total of 109 of the 253 patients (43%) required angioembolization to control arterial bleeding.

The images were axial in orientation with either 1.5 mm or 3 mm reconstruction thickness. Manual labeling was performed by one board-certified radiologist with 7 years of dedicated experience in trauma imaging. Labeling of hematoma was performed using 3D Slicer (version 4.8.1, www.slicer.org) with the spherical paint tool thresholded between -20 and 100 Hounsfield Units. This allowed segmentation within the range of hematoma, accounting for lower pixel values from image noise while avoiding fat. A small (3–5 mm) region of interest (ROI) was used to delineate the interface with structures with overlapping density including pelvic organs and muscle. Larger ROIs (up to 20 mm) were used elsewhere. Quality check by a second board-certified radiologist with 3 years of experience involved careful inspection for errors and editing as needed.

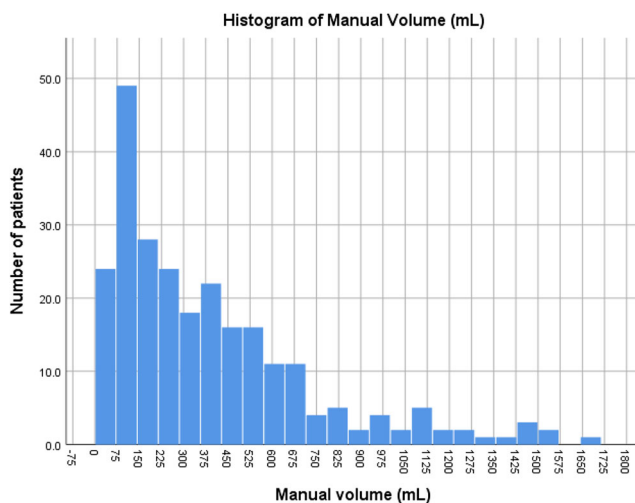


Fig. 1 Histogram showing distribution of manual volumes by number of patients

Image and Label Preprocessing

Both the DICOM images and ground truth masks were converted to NIFTI format. All axial images and manually labeled masks were resampled to 1 mm section thickness and reconstructed in sagittal and coronal planes, yielding an isotropic volume. Following resampling, the corpus consisted of a total of 447,238 images with a 512×512 matrix. No other preprocessing steps were performed.

Deep Learning Method: Recurrent Saliency Transformation Network

A flow diagram of the recurrent saliency transformation network (RSTN) implemented for pelvic hematoma segmentation is shown in Fig. 2a. A detailed technical explanation of RSTN is offered in the work of Yu et al. RSTN is a modification of the coarse-to-fine algorithm (C2F) described by Zhou et al. that uses 2D-FCNs in three planes (axial, coronal, and sagittal) for training and inference [23]. The algorithm first employs a coarse-scaled U-Net-based network with the entire volume as its input to localize smaller volumes of interest. The coarse segmentation is used to automatically generate a bounding box around which the image is cropped, and this volume is then fed to a fine-scaled U-Net-based network that achieves dense segmentation of fine details within the smaller volume. The results of FCNs from the three planes are fused [23]. Within each plane, FCN prediction is based on three consecutive slices. This three-slice segmentation model optimizes training from contextual cues in neighboring slices. In RSTN, improved preservation of large-scale contextual cues and fine spatial dependencies is achieved by simultaneous optimization of coarse and fine images using a global Dice loss function and use of a “saliency transformation module” in the coarse stage [28]. The saliency transformation module repeatedly transforms the segmentation probability map from previous iterations of the coarse-scaled FCN as spatial priors, resulting in a more refined segmentation in the coarse stage that enhances dense segmentation by the downstream fine-scaled FCN [28]. The method has similar advantages to recurrent neural networks for retaining local and global information by propagating label masks through multiple iterations [30–32], however in RSTN, training is end-to-end using simultaneous coarse and fine inputs [28]. The saliency transformation module and joint optimization of coarse and fine-scaled images using a single Dice loss function enhance learning based on both global contextually rich information and fine spatial dependencies [28]. The U-Net-like FCN base architecture used for both coarse and fine segmentations has a collapsing arm that uses a series of 3×3 convolutional filters with initial stride length of 1, input matrix size of $512 \times 512 \times 3$, and padding of 100. The architecture consists of blocks of convolutional layers followed by ReLU activation and max-

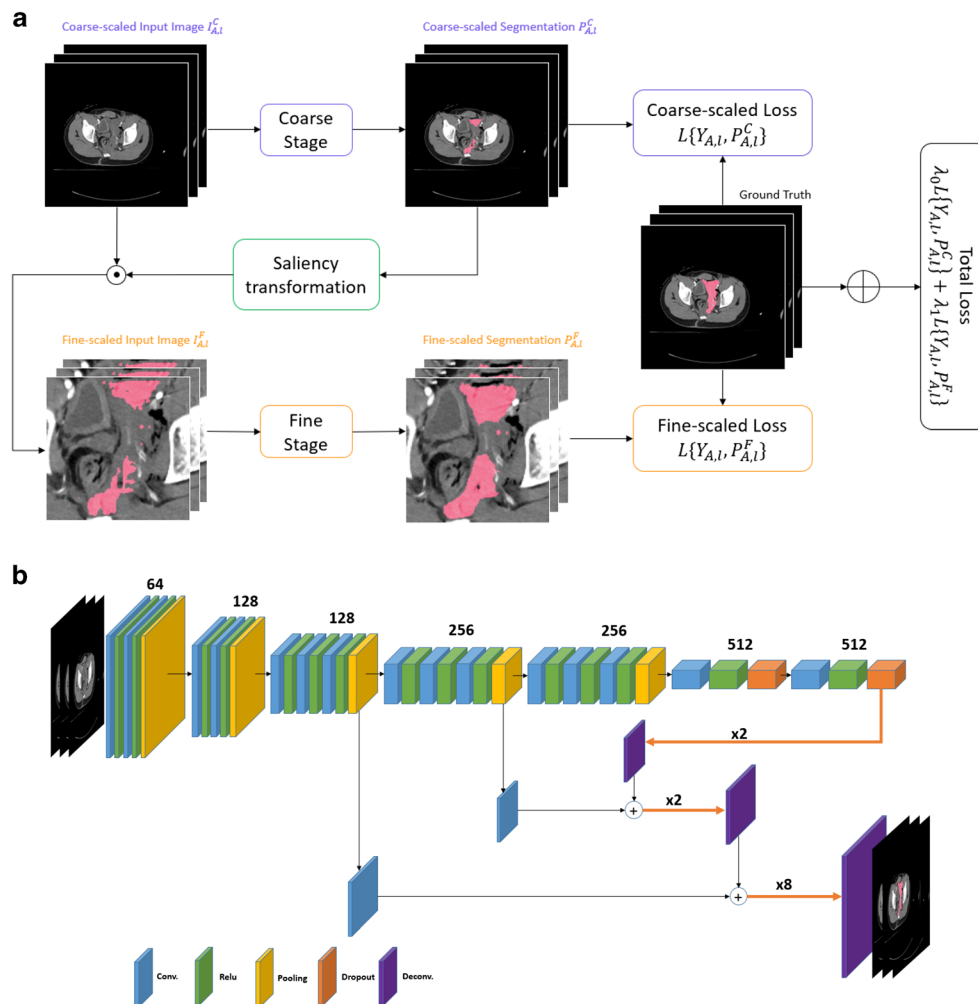


Fig. 2 **a** RSTN adapted for pelvic hematoma segmentation. RSTN is a coarse-to-fine deep learning method that employs two identical sequential U-Net-like networks (base architecture is shown in **b**). Initially, the entire volume is used as input for the coarse network and the coarse segmentation is then used to localize smaller volumes of interest. A bounding box is generated around the coarse segmentation and the volume is cropped. The cropped volume is then fed to the fine-scaled network to achieve dense segmentation of fine details within the smaller volume. Within each plane, FCN prediction is based on three consecutive slices. This three-slice segmentation model optimizes training from contextual cues in neighboring slices. The results of FCNs from the three planes are fused using majority voting [23]. During the training phase (shown), the saliency transformation module repeatedly transforms the coarse-scaled segmentation probability map from previous iterations of coarse-scaled segmentation as spatial priors resulting in a more refined input that enhances

pooling, with dropout and deconvolutions (upsampling) in deeper layers (see Fig. 2b). The final convolutional layer uses sigmoid activation for pixelwise classification.

The algorithm was developed in Python (version 3.6.6). The PyTorch (version 0.4.0) deep learning platform was employed for training and validation using our bleeding pelvic fracture dataset. All experiments were performed using a Titan Xp GPU with 12 GB of memory, running on Ubuntu. The

subsequent fine-scaled segmentation [28]. The fine and coarse-scaled U-Net-based segmentations are jointly optimized by a single global Dice loss function (see formula for total loss, right). **b** FCN base architecture used during both coarse- and fine-stage segmentation. The FCN architecture has five major downsampling blocks, with each block consisting of 2–3 convolution modules (3×3 kernels with ReLU activation), followed by 1 max-pooling layer (2×2 kernels). In addition, three major upsampling blocks are employed where the first two deconvolution layers use 4×4 kernels with a stride of two and the last deconvolution uses 16×16 kernels with a stride of eight. Skip connections are used to combine the low-level and high-level features for better localization quality. The final convolutional layer uses a 1×1 kernel with sigmoid activation. Both the input and the output are of the same 512×512 resolution. Prediction is based on three consecutive slices, which optimizes training from contextual cues in neighboring slices

RSTN network was previously initialized using weights from prior work on the PascalVOC image segmentation task [16, 28]. The network base architecture configuration and all hyperparameters were inherited from work by Yu et al. using RSTN for pancreas segmentation [28]. The network was trained using six epochs, with a learning rate of 10^{-5} for the first five epochs, followed by 10^{-6} during for a 6th epoch, with a minibatch size of 1. For training and validation, fivefold

cross-validation was employed with the implementation using an 80% training, 20% validation split (i.e., the model was trained on four of the five subsets and tested on the remaining subset for each of the five possible combinations). As there is no published prior art for comparison, fivefold cross-validation Dice similarity coefficient results of pelvic hematoma segmentation using the Recurrent Saliency Transformation Network were compared using the same pelvic fracture dataset to 1) the coarse to fine network architecture without the saliency transformation module, and 2) a publicly available 3D U-Net implementation from the Deep Learning Tool Kit (DLTK) [33], which provides popular baseline reference implementations for efficient experimentation tailored to medical image analysis (3D U-Net implementation details follow work by Ronneberger, He, and Cicek [14, 34, 35]).

Statistical Analysis

Segmentation Accuracy

Summary statistics for segmentation accuracy included voxel by voxel comparisons of spatial overlap using the Dice similarity coefficient (DSC), defined as:

$$\text{DSC} = \frac{2 \text{ TP}}{2 \text{ TP} + \text{FP} + \text{FN}}$$

Where true positive (TP), true negative (TN), false positive (FP), and false negative (FN)—predicted segmentations for each voxel are compared to the manual ground truth label. The closer the value to 1, the greater the segmentation overlap, with a value of 1 indicating perfect overlap.

Volumetric Comparisons

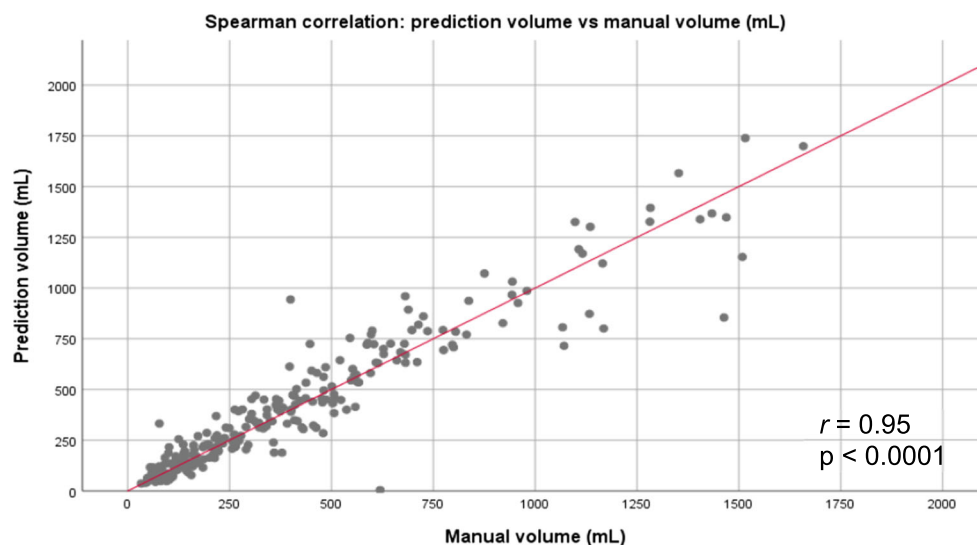
Ultimately, volumes alone are used for clinical prediction. The Pearson's coefficient (r) was used to assess correlations between manual and predicted RSTN segmentations. Comparison of means was performed using Student's t test. The between method similarity of manual and RSTN-generated volumes was assessed with the single-measures intraclass correlation coefficient (ICC), with $\text{ICC} > 0.75$ considered to indicate excellent concordance [36]. Measurement bias and 95% limits of agreement were interrogated using Bland-Altman plots. One-way analysis of variance (ANOVA) was used to compare Dice similarity coefficients between the three Tile groups to assess whether the degree of pelvic distortion affected RSTN segmentation accuracy. Finally, accuracy of prediction of major bleeding requiring angioembolization was assessed for both manual and automated RSTN volume measurements using ROC analysis, with p values for comparisons determined using the Hanley-McNeil method [37]. All

volumetric analyses were performed using SPSS Statistics version 25 (IBM corporation; Armonk, NY).

Results

We achieved a mean Dice similarity coefficient for RSTN of 0.71 (\pm SD of 0.10) for predicted segmentation of pelvic hematomas in fivefold cross-validation. The mean DSC of RSTN compared favorably to results obtained for the coarse to fine network with the saliency transformation module removed (DSC of 0.65 ± 0.12) and using a DLTK baseline reference 3D U-Net architecture [33] (DSC of 0.49 ± 0.16). The mean inference time for RSTN segmentation in the five validation groups was 0.90 min (\pm SD of 0.26). Pearson's correlation between manual ground truth label volumes and predicted volumes using RSTN are shown in Fig. 3. Bland-Altman plot showing measurement bias and 95% limits of agreement are shown in Fig. 4. AUC curves for manual and automated RSTN-derived volumes for predicting major arterial injury requiring angioembolization are presented in Fig. 5. Visual results are illustrated in Figs. 6 and 7. Qualitatively, the predicted RSTN segmentations appear highly concordant with manual segmentations despite the markedly irregular nature and variable locations of hematomas. Pelvic viscera and musculature of the pelvic floor, sidewall, and suprapubic space were routinely avoided in the predicted labels despite substantial displacement and distortion of these anatomic structures by space-occupying hematoma and pelvic ring disruptions. Mean manual hematoma volume measurements were ($390.5 \text{ mL} \pm \text{SD of } 342.5 \text{ mL}$) and mean predicted volumes were ($399.9 \pm \text{SD of } 344.8$) ($p = 0.76$). Correlations between manual and predicted label volumes were strong and highly significant ($r = 0.948$; $p < 0.0001$; see Fig. 2). Measurement bias between manual and predicted hematoma volumes was low (9.4 mL over-measurement in predicted labels), 95% limits of agreement were relatively narrow (-227.9 to 209.1 mL), and between-method intraclass correlation coefficient for manual and predicted volumes was in the excellent range ($\text{ICC} = 0.95$; 95% confidence interval 0.93–0.96). The Dice score showed a statistically significant but weak increase (Pearson's $r = 0.29$, $p < 0.0001$) proportional to the size of hematoma (i.e., larger hematomas had slightly improved Dice scores overall), which has clinical relevance since larger hematomas correspond with more dire outcomes and greater probabilities of requiring urgent angioembolization, while small hematomas are managed conservatively. In principle, less accurate segmentations are not as important with small hematomas, provided that volume measurements correlate closely with manual segmentations (see Fig. 2). There was no significant difference in Dice scores between the three Tile grades of pelvic instability using ANOVA ($p = 0.11$). AUCs for predicting major arterial injury requiring

Fig. 3 Scatter matrix of manual label volumes (x-axis) plotted against RSTN-predicted label volumes (y-axis) with best-fit line. Pearson correlation between manual and predicted hematoma volumes was very strong ($r = 0.95$) and highly significant ($p < 0.0001$)



angioembolization was 0.80 with manual segmentation versus 0.81 with the automated method ($p = 0.92$).

Discussion

Manual and semi-automated methods for pelvic hematoma segmentation have been described and clinically validated. Despite evidence that pelvic hematoma volumes are the strongest independent predictor of major arterial injury, widespread point of care use is precluded either by time effort involved or lack of widespread familiarity with semi-automated techniques. Typically, volumes are instead assessed heuristically

using coarse terms (e.g., small, medium, or large). Human prediction of major arterial bleeding has suboptimal accuracy and is highly subjective. To our knowledge, our work represents the first fully automated algorithm for segmentation of traumatic pelvic hematomas. The automated method results in reliable and objective volumetric measurements which are qualitatively acceptable, avoiding viscera and muscle even with substantial distortions. Automated and manual volume measurements had excellent between-method intraclass correlation (0.95) with minimal measurement bias (-9.39 mL), and AUCs for predicting angioembolization need that are not significantly different from manual measurements (AUC 0.81—automated versus 0.81 manual, $p = 0.92$). There was no

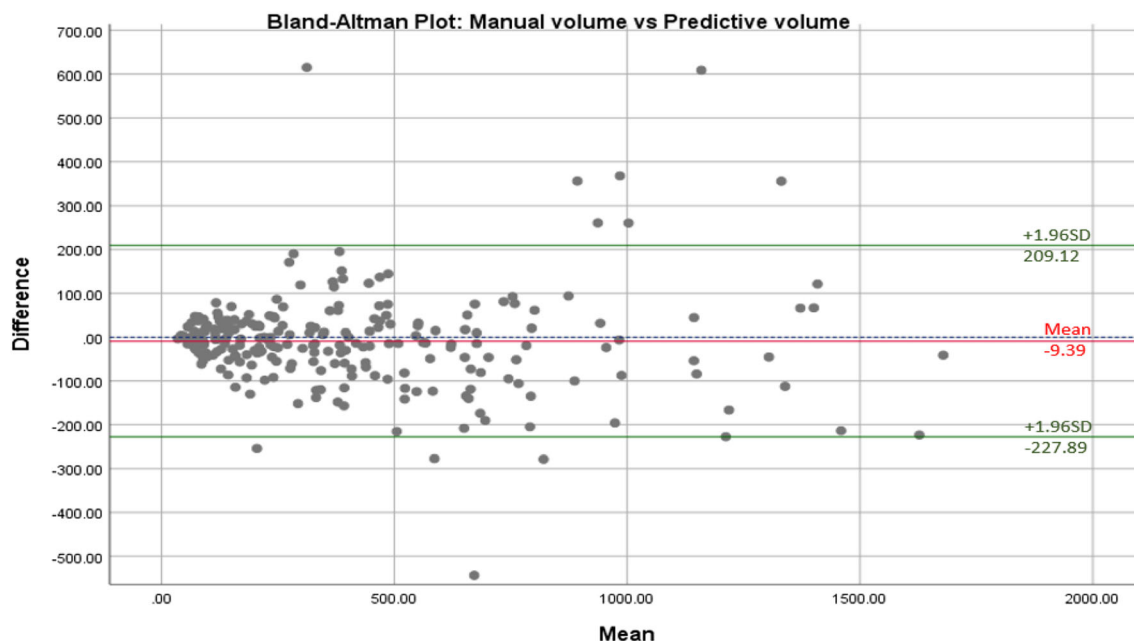


Fig. 4 Bland-Altman plot demonstrates minimal over-measurement bias for predicted RSTN labels (9.4 mL difference between predicted and manual), with 95% limits of agreement of -227.9 and 209.1 mL

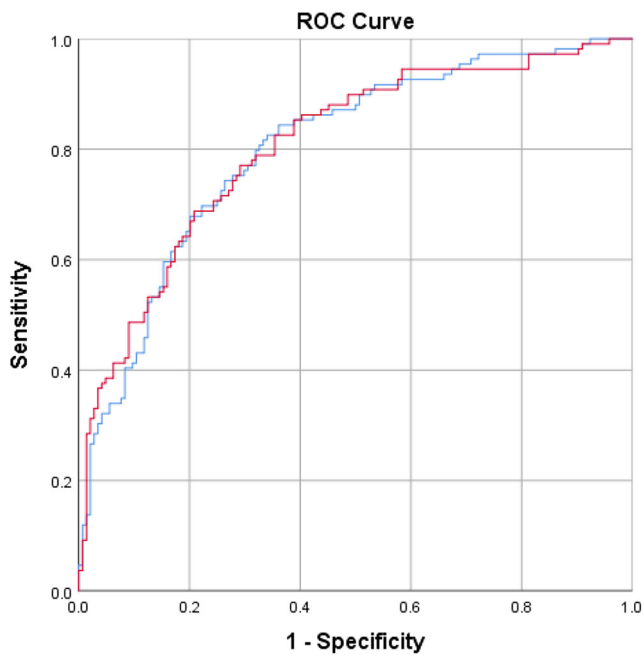


Fig. 5 Area under the receiver operating characteristic curves (AUCs) of hematoma volume for predicting major arterial injury requiring angioembolization are shown. AUC for manual volumes (blue) was 0.80 and AUC for automated RSTN volumes (red) was 0.81, with no significant difference in performance between the two groups ($p = 0.92$)

significant difference between groups based on degree of instability using ANOVA analysis ($p = 0.11$), suggesting that the degree of pelvic ring distortion did not have a meaningful effect on algorithm performance.

Future Avenues

Our hematoma segmentation method can be modified and trained to detect sources of hemorrhage in other body regions but is currently meant to be applied only in patients with pelvic fractures. We have begun development of detection algorithms to first identify pelvic fractures on CT. The algorithms could then be incorporated into an imaging analytics pipeline that could improve the clinical workflow in a number of ways. Once developed, we propose to deploy the algorithms onto a secure cloud- or workstation-based virtual

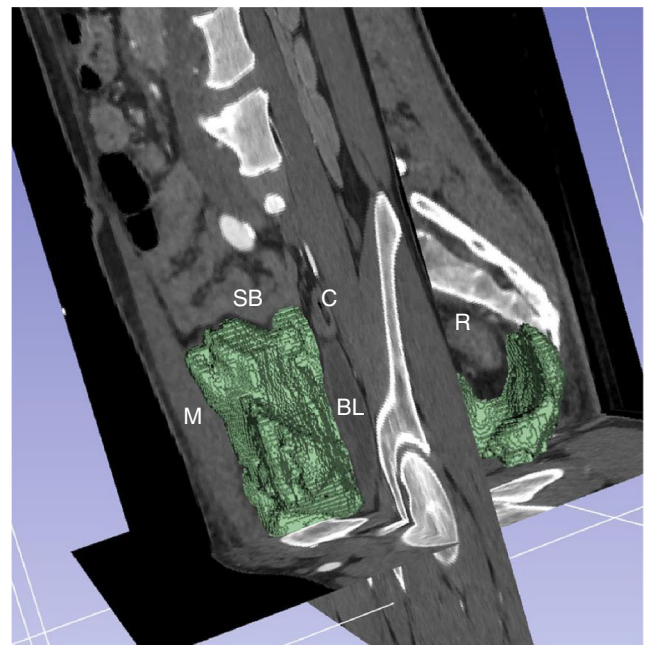


Fig. 7 3D surface rendering of automated RSTN prediction label superimposed on the CT dataset, displayed in three orthogonal planes in a 42-year-old man following a motorcycle collision (DSC = 0.85, manual volume = 316.5 mL; automated volume = 334.9 mL). The patient was managed conservatively. Notice that the label avoids the displaced bladder (BL), rectus abdominis muscle (M), colon (C), small bowel (SB), and rectum (R)

machine client platform [38]. The algorithms would preprocess all CT scans that include the pelvis sent to the client based on trauma resuscitation unit ordering location. This could trigger alerts for our trauma radiologists and surgeons when a patient is at high risk for life-threatening bleed or prioritize studies in the unread worklist according to the size of predicted hematoma, which may substantially decrease time to intervention in the emergent trauma setting. We also plan to assess generalizability of our algorithm to other institutions and scan parameters (e.g., different CT makes and models, reconstruction algorithms, filters, and slice thickness) in a multicenter study. Clinical impact could then be measured based on interpretation turnaround times, time to intervention, patient outcome, and cost-effectiveness. The ability to visualize and even interactively fine-tune the predicted segmentation is another



Fig. 6 Axial images through traumatic pelvic hematoma in a 79-year-old man following a motor vehicle collision (RSTN DSC = 0.86; manual volume = 1287.7 mL; automated volume = 1327.0). The patient

underwent angioembolization for arterial bleeding. The automated prediction label closely follows the contours of the hematoma, avoiding muscle, viscera, and bone

important workflow option that would potentially improve precision and provide additional training data to further refine the algorithm. Quantitative assessment of change over time could also be made with repeat scans to determine whether a pelvic hematoma is changing in size and may warrant re-intervention. Increasingly accurate clinical prediction might be achieved by incorporating multiple volumetric features including contrast extravasation, pelvic fracture grade, and features of body composition along with clinical and laboratory values [9, 39, 40].

Quantitative imaging research, mature in other areas, has received relatively little attention in abdominopelvic trauma as measurements of hemorrhage volumes, which can exceed 1 L after severe injuries, are labor intensive, and previously without a clear avenue toward practical point-of-care use [8]. The automated algorithm also has the potential to accelerate clinically relevant scientific discovery for CT-based outcome prediction in pelvic trauma and objective measurements will allow meaningful comparison between scientific studies. The relatively robust results of our method are expected to have broader implications such as for automated segmentation of hemoperitoneum after solid organ injuries, and segmentation of abdominal free fluid from a variety of non-traumatic pathologies including perforated bowel, pancreatitis, abdominal compartment syndrome, and ascites in cirrhotic patients.

References

1. Yoon W, Kim JK, Jeong YY, Seo JJ, Park JG, Kang HK: Pelvic arterial hemorrhage in patients with pelvic fractures: Detection with contrast-enhanced CT. *Radiographics*. 24(6):1591–1605, 2004
2. Demetriades D, Karaiskakis M, Toutouzas K, Alo K, Velmahos G, Chan L: Pelvic fractures: Epidemiology and predictors of associated abdominal injuries and outcomes. *Journal of the American College of Surgeons* 195(1):1–10, 2002
3. Holstein JH, Culemann U, Pohlemann T, WGMiPF P: What are predictors of mortality in patients with pelvic fractures? *Clinical Orthopaedics and Related Research*. 470(8):2090–2097, 2012
4. Heckbert SR, Vedder NB, Hoffman W, Winn RK, Hudson LD, Jurkovich GJ, Copass MK, Harlan JM, Rice CL, Maier RV: Outcome after hemorrhagic shock in trauma patients. *Journal of Trauma and Acute Care Surgery*. 45(3):545–549, 1998
5. Sathy AK, Starr AJ, Smith WR, Elliott A, Agudelo J, Reinert CM, Minei JP: The effect of pelvic fracture on mortality after trauma: An analysis of 63,000 trauma patients. *JBJS*. 91(12):2803–2810, 2009
6. Dreizin D, Munera F: Blunt polytrauma: Evaluation with 64-section whole-body CT angiography. *Radiographics*. 32(3):609–631, 2012
7. Cullinane DC, Schiller HJ, Zielinski MD, Bilaniuk JW, Collier BR, Como J, Holevar M, Sabater EA, Sems SA, Vassy WM, Wynne JL: Eastern Association for the Surgery of Trauma practice management guidelines for hemorrhage in pelvic fracture—Update and systematic review. *Journal of Trauma and Acute Care Surgery*. 71(6):1850–1868, 2011
8. Blackmore CC, Jurkovich GJ, Linnau KF, Cummings P, Hoffer EK, Rivara FP: Assessment of volume of hemorrhage and outcome from pelvic fracture. *Archives of surgery*. 138(5):504–509, 2003
9. Dreizin D, Bodanapally U, Boscak A, Tirada N, Issa G, Nascone JW, Bivona L, Mascarenhas D, O’Toole RV, Nixon E, Chen R, Siegel E: CT prediction model for major arterial injury after blunt pelvic ring disruption. *Radiology*. 287(3):1061–1069, 2018
10. Dreizin D, Bodanapally UK, Neerchal N, Tirada N, Patlas M, Herskovits E: Volumetric analysis of pelvic hematomas after blunt trauma using semi-automated seeded region growing segmentation: A method validation study. *Abdominal Radiology*. 41(11):2203–2208, 2016
11. Litjens G, Kooi T, Bejnordi BE, Setio AAA, Ciompi F, Ghafoorian M, van der Laak JAWM, van Ginneken B, Sánchez CI: A survey on deep learning in medical image analysis. *Medical image analysis*. 42:60–88, 2017
12. Krizhevsky A, Sutskever I, Hinton GE: Imagenet classification with deep convolutional neural networks. In: *Advances in neural information processing systems 2012*, pp. 1097–1105
13. Chartrand G, Cheng PM, Vorontsov E, Drozdal M, Turcotte S, Pal CJ, Kadoury S, Tang A: Deep learning: A primer for radiologists. *Radiographics*. 37(7):2113–2131, 2017
14. Ronneberger O, Fischer P, Brox T: U-net: Convolutional networks for biomedical image segmentation. *International Conference on Medical image computing and computer-assisted intervention: Springer*:234–241, 2015
15. Milletari F, Navab N, Ahmadi S-A: V-net: Fully convolutional neural networks for volumetric medical image segmentation. *3D vision (3DV)*, 2016 fourth international conference on. *IEEE*, 2016, pp. 565–571
16. Long J, Shelhamer E, Darrell T.: Fully convolutional networks for semantic segmentation. *Proceedings of the IEEE conference on computer vision and pattern recognition 2015*; p. 3431–3440.
17. Yasaka K, Akai H, Abe O, Kiryu S: Deep learning with convolutional neural network for differentiation of liver masses at dynamic contrast-enhanced CT: A preliminary study. *Radiology*. 286(3):887–896, 2017
18. Christ PF, Elshaer MEA, Ettliger F et al.: Automatic liver and lesion segmentation in CT using cascaded fully convolutional neural networks and 3D conditional random fields. *International Conference on Medical Image Computing and Computer-Assisted Intervention: Springer*:415–423, 2016
19. Yang D, Xu D, Zhou SK, et al. Automatic liver segmentation using an adversarial image-to-image network. *International Conference on Medical Image Computing and Computer-Assisted Intervention: Springer*, 2017; p. 507–15.
20. Roth HR, Lu L, Farag A et al.: Deeporgan: Multi-level deep convolutional networks for automated pancreas segmentation. In: *International conference on medical image computing and computer-assisted intervention*. Springer, 2015, pp. 556–564
21. Roth HR, Farag A, Lu L, Turkbey EB, Summers RM.: Deep convolutional networks for pancreas segmentation in CT imaging. *Medical Imaging 2015: Image Processing: International Society for Optics and Photonics*, 2015; p. 94131G.
22. Zhou Y, Xie L, Fishman EK, Yuille AL: Deep supervision for pancreatic cyst segmentation in abdominal CT scans. *International conference on medical image computing and computer-assisted intervention*. Springer, 2017, pp. 222–230
23. Zhou Y, Xie L, Shen W, Wang Y, Fishman EK, Yuille AL: A fixed-point model for pancreas segmentation in abdominal CT scans. In: *International conference on medical image computing and computer-assisted intervention*. Springer, 2017, pp. 693–701
24. Yu L, Yang X, Chen H, Qin J, Heng P-A: Volumetric ConvNets with mixed residual connections for automated prostate segmentation from 3D MR images. *AAAI 2017*, pp. 66–72

25. Kohl S, Bonekamp D, Schlemmer H-P, et al. Adversarial networks for the detection of aggressive prostate cancer. arXiv preprint arXiv:170208014. 2017.
26. Dreizin D, Bodanapally U, Mascarenhas D et al.: Quantitative MDCT assessment of binder effects after pelvic ring disruptions using segmented pelvic haematoma volumes and multiplanar caliper measurements. *European radiology*:1–10, 2018
27. Dreizin D, Nascone J, Davis DL, Mascarenhas D, Tirada N, Chen H, Bodanapally UK: Can MDCT unmask instability in binder-stabilized pelvic ring disruptions? *American Journal of Roentgenology*. 207(6):1244–1251, 2016
28. Yu Q, Xie L, Wang Y, Zhou Y, Fishman EK, Yuille AL: Recurrent saliency transformation network: Incorporating multi-stage visual cues for small organ segmentation. *Conference on Computer Vision and Pattern Recognition (CVPR)*, 2018
29. Elzik ME, Dirschl DR, Dahners LE: Correlation of transfusion volume to change in hematocrit. *American journal of hematology*. 81(2):145–146, 2006
30. Dou Q, Chen H, Jin Y, Yu L, Qin J, Heng P-A: 3D deeply supervised network for automatic liver segmentation from CT volumes. *International Conference on Medical Image Computing and Computer-Assisted Intervention: Springer*:149–157, 2016
31. Harrison AP, Xu Z, George K, Lu L, Summers RM, Mollura DJ.: Progressive and multi-path holistically nested neural networks for pathological lung segmentation from CT images. *International Conference on Medical Image Computing and Computer-Assisted Intervention: Springer*, 2017; p. 621–9.
32. Roth HR, Lu L, Farag A, Sohn A, Summers RM: Spatial aggregation of holistically-nested networks for automated pancreas segmentation. *International conference on medical image computing and computer-assisted intervention*. Springer, 2016, pp. 451–459
33. Pawlowski N, Ktena SI, Lee MC et al.: Dltk: State of the art reference implementations for deep learning on medical images. arXiv preprint arXiv:171106853, 2017
34. He K, Zhang X, Ren S, Sun J: Identity mappings in deep residual networks. *European conference on computer vision: Springer*:630–645, 2016
35. Çiçek Ö, Abdulkadir A, Lienkamp SS, Brox T, Ronneberger O: 3D U-net: Learning dense volumetric segmentation from sparse annotation. In: *International conference on medical image computing and computer-assisted intervention*. Springer, 2016, pp. 424–432
36. Cicchetti DV: Guidelines, criteria, and rules of thumb for evaluating normed and standardized assessment instruments in psychology. *Psychological assessment*. 6(4):284–290, 1994
37. Hanley JA, McNeil BJ: A method of comparing the areas under receiver operating characteristic curves derived from the same cases. *Radiology*. 148(3):839–843, 1983
38. EnvoyAI launches with 35 algorithms contributed by 14 newly-contracted artificial intelligence development partners. *Global newswire*. CAMBRIDGE, Mass.2017.
39. Dreizin D: Segmented pelvic hematoma volumes, intravenous contrast extravasation volumes, and extravasation rate are all independently predictive of major arterial injury after pelvic fracture: Analysis of a prospective cohort. *Radiologic Society of North America 104th Scientific Assembly and Annual Meeting*2018
40. Dreizin D, Chen R, Rosales R, Li G, Bodanapally U.: Volumetric Markers of Body Composition Improve Personalized Prediction of Major Arterial Bleeding after Blunt Pelvic Ring Disruption. *American Society of Emergency Radiology Annual Scientific Meeting and Postgraduate Course*. McLean, Virginia: Springer-Verlag, 2018; p. 565–611.

Publisher's Note Springer Nature remains neutral with regard to jurisdictional claims in published maps and institutional affiliations.